Integral Field Spectroscopy of Planetary Nebulae with MUSE

Jeremy R. Walsh [1,*] and **Ana Monreal-Ibero** [2,3]

1   European Southern Observatory, 85748 Garching, Germany
2   Instituto de Astrofísica de Canarias (IAC), E-38205 La Laguna, Tenerife, Spain; amonreal@iac.es
3   Dpto. Astrofísica, Universidad de La Laguna, E-38206 La Laguna, Tenerife, Spain
*   Correspondence: jwalsh@eso.org

Abstract: The Multi-Unit Spectroscopic Explorer (MUSE) is a large integral field unit mounted on the ESO Very Large Telescope. Its spatial (60 arcsecond field) and wavelength (4800–9300Å) coverage is well suited to detailed imaging spectroscopy of extended planetary nebulae, such as in the Galaxy. An overview of the capabilities of MUSE applied to Planetary Nebulae (PNe) is provided together with the specific advantages and disadvantages. Some examples of archival MUSE observations of PNe are provided. MUSE datacubes for two targets (NGC 3132 and NGC 7009) are analyzed in detail, and they are used to show the advances achievable for planetary nebula studies. Prospects for further MUSE observations of PNe and a broader analysis of existing datasets are outlined.

1. Overview of MUSE

The Multi-Unit Spectroscopic Explorer (MUSE) is a large field-of-view ($\sim$60 $\times$ 60$''$) optical integral field spectrometer mounted on the European Southern Observatory (ESO) Very Large Telescope (VLT), currently on Unit Telescope 4 (Yepun). The field is divided into 24 slices, and each is sent to a separate integral field unit (IFU) that divides the sub-field into 48 mini slits, which are all fed to one of the 24 identical spectrometers [1]. Each spectrometer module is equipped with a volume phase holographic grating covering the full wavelength range 4600–9300Å and imaged by an EEVdeep depletion, anti-reflection-coated 4k $\times$ 4k Charge Coupled Detector (CCD). Details of the instrument can be found on the ESO MUSE web page (http://www.eso.org/sci/facilities/paranal/instruments/muse/inst.html) and in the MUSE Instrument Manual [2].

Although the instrument format is fixed in terms of the number of slicers and spectrographs, there are some options for feeding the field from the VLT to the instrument and one wavelength range choice. Table 1 lists the various options. In Wide Field Mode (WFM), the full field of 300 $\times$ 300 pixels, each 0.20 $\times$ 0.2$''$, is covered. Using the VLT Deformable Secondary Mirror (DSM), a Ground Layer Adaptive Optics (AO) feed is available, which provides the same field, but an improved image quality (typically $\times$2 ensquared energy, but depending on atmospheric conditions). Higher spatial resolution is achievable with laser tomographic AO, and the field size is reduced to 7.5$''$ (Narrow Field Mode (NFM)). It should be noted that, since a sodium laser is employed for the AO modes, the spectral region around the Na I doublet (58905896Å) is blocked by a filter. In both WFM and NFM, an alternative wavelength range can be assessed (called extended mode), which shifts the blue cut-off from 4800 to 4650Å; however, this mode suffers second order contamination at wavelengths above 8000Å. Most of these modes have been employed for MUSE observations of PNe.

Table 1. The Multi-Unit Spectroscopic Explorer's (MUSE) instrumental parameters. AO, Adaptive Optics.

Mode	Field ($''$)	Pixel ($''$)	Image Quality
Wide Field Mode (WFM)	59.9×60.0	0.20	Native seeing
Wide Field Mode + AO	59.9×60.0	0.20	$\gtrsim 2\times$ encircled energy
Narrow Field Mode (NFM)	7.42×7.43	0.025	55–80 milli-arcseconds

Spectral mode	Wavelength range (Å)	Resolving power	Field mode
Normal (N)	4800–9300	1770–3590	WFM
Normal (N)	4800–5780, 6050–9300	1740–3450	NFM
Extended (E)	4650–9300	1770–3590	WFM
Extended (E)	4650–5760, 6010–9300	1740–3450	NFM

2. Suitability of MUSE for PNe

Planetary nebulae are extended emission and continuum nebulae ionized by a central hot star, mostly representing the shell of gas ejected during the previous Asymptotic Giant Branch (AGB) phase of the evolution of a 0.8–8.0 $M_\odot$ star. PNe in the Galaxy present projected sizes from fractions of an arcsecond for compact and/or distant PNe to almost half a degree, making them good targets for IFU observation (e.g., [3]). MUSE with its large IFU field can be considered well matched to spectral imaging of a range of Galactic PNe. For nebulae where the emission outskirts of the field are contained within the MUSE field, direct sky removal is facilitated; nebulae much larger can be effectively sky subtracted using an offset sky exposure. Details of the compact structures in larger nebulae, or more compact PNe, are well accessible to the narrow field mode. The native spaxel size of $0.20''$ is matched to sampling good Paranal seeing ($\sim 0.5''$), and smaller scale structures can be imaged in detail; while NFM competes with Hubble Space Telescope imaging to the $0.1''$ level.

The spectral coverage of MUSE provides a good sampling of the rich optical emission spectrum consisting of recombination and collisionally excited lines, which have been observed over many decades and have contributed a substantial literature on the lines, their parent atoms and ionization mechanisms, and their use as diagnostics of physical processes (e.g., [4–6]). The applicability of diagnostic line ratios for dust extinction, electron density (N_e), and temperature (T_e) measurement and for abundance determination, refined through observations of PNe, have been applied to ionized regions in galaxies at the highest observed redshifts. The MUSE coverage to 9300Å allows the Paschen continuum jump of ionized H (and ionized He) at ~ 8210Å [7] to be measured (although compromised in extended mode by second order contamination), providing another temperature and density probe distinct from those of the emission lines.

The wavelength compass does however bring some disadvantages compared to full optical (3500–10,000Å) and higher resolution spectroscopy:

- the spectral Resolving power (R) is relatively low ($\sim$1800–3600; see Table 1), thus not sampling the emission lines at the optimal value of two times their intrinsic (thermal and Doppler broadened) width (R > 10,000). On multiple sampled spectra, some restoration is of course possible to assess line blends below 3–4Å separation;
- Important diagnostic lines blueward of 4650Å are not included, including the [O II] doublet (3726,3729Å) for N_e measurement, [Ne III] lines, and the auroral [O III]4363Å, which, by the ratio to the [O III]4959,5007Å lines, provides T_e for the higher ionization medium. Alternative, less bright diagnostic lines are available in the MUSE range, involving less major coolants of the gas, such as N_e from [S II] 6716/6731Å, [Cl III] 5517/5537Å, and [Ar IV] 4711/4740Å in extended mode, T_e from [O I] 6302/5577Å, [N II] 6583/5755Å, [S III] 9069/6311Å, and [Ar III] 7135/5192Å, thus partially compensating for the absence of the "classical" O^{++} diagnostic, which samples the bulk ionization component for all but the lowest ionization PNe;

- The bright and important (at least for higher ionization PNe) He II 4686Å line is missing from the MUSE normal mode (but included in extended mode). This absence is partially compensated by the He II 5411Å line, although ~10 times fainter;
- The [O II]7319,7320Å and 7329,7330Å doublet is much fainter than the blue [O II]3726,3729Å lines, but can be used for the determination of the O^+ ionic fraction;
- Relatively few Optical metal Recombination Lines (ORLs) are covered in normal mode (mostly N), and while the 4650Å region important for the brightest O II recombination lines is just included in extended mode, no Ne ORLs are available.

3. Archival MUSE Observations of PNe

Some 20 PNe have been observed with MUSE to data at various phases of the instrument commissioning and also in guest observer (open) time. Table 2 lists the PNe observed with an indication of the mode(s) employed. Data for only two PNe (NGC 3132 and NGC 7009; see the next section) have been published to date, reflecting the large analysis task associated with these rich datasets encompassing hundreds of detectable emission lines per spaxel.

Table 2. Multi-Unit Spectroscopic Explorer (MUSE) archival observations of planetary nebulae. Comm., Commissioning.

Target	Designation	MUSE Mode	Obs.Type	Notes
NGC 6369	PNG002.4 +05.8	WFM AO, N	Comm.	
M 1-42	PNG 002.7 −04.8	WFM, E	GO	ESO Proposal 097.D-0241
Hf 2-2	PNG 005.1 −08.9	WFM, E	GO	097.D-0241
GJJC 1	PNG 009.8 −07.5	NFM, N	Comm.	IRAS 18333-2357
Sa 3-151	PNG 033.2 −01.9	NFM, N	Comm.	
NGC 6778	PNG 034.5 −06.7	WFM AO, N	Comm.	
NGC 7009	PNG 037.7 −34.5	WFM, N	SV	Walsh et al. (2016,2018)
NGC 7009	PNG 037.7 −34.5	WFM, E	GO	097.D-0241
NGC 7009	PNG 037.7 −34.5	NFM, N	Comm.	
Abell 46	PNG 055.4 +16.0	WFM, E	GO	097.D-0241
IC 418	PNG 215.2 −24.2	WFM, N	Comm.	
NGC 3242	PNG 261.0 +32.0	WFM, E	GO	097.D-0241
NGC 2818	PNG 261.9 +08.5	WFM, N	Comm.	
NGC 3132	PNG 272.1 +12.3	WFM, N	Comm.	Monreal-Ibero and Walsh (2020)
IC 2501	PNG 281.0 −05.6	WFM, N	Comm.	
NGC 4361	PNG 294.1 +43.6	WFM, N	Comm.	
NGC 5189	PNG 307.2 −03.4	WFM, N	Comm.	
IC 4406	PNG 319.6 +15.7	WFM, N	Comm.	Type I PN; see Figure 1
Mz-3	PNG 331.7 −01.0	NFM, N	Comm.	
CPD-56 8032	PNG 332.9 −09.9	NFM, N	Comm.	He 3-1333
NGC 6153	PNG 341.8 +05.4	WFM, E	GO	097.D-0241
NGC 6563	PNG 358.5 −07.3	WFM AO, N	Comm.	See Figure 1

Many PNe were observed as part of the Commissioning (Comm.) of the instrument at various stages (Comm. entries in Table 2), reflecting the fact that they make excellent press release images and enable the capabilities of the instrument to be thoroughly exercised (extended and point sources, line and continuum spectra with many emission lines, some with fixed ratios). Figure 1 shows images from the ESO Release (eso1724 https://www.eso.org/public/news/eso1724/) of some of these PNe observed with WFM and GLAO, well illustrating the quality of the imaging data that can be extracted from the position–wavelength reduced cubes. IC 4406 is a Type I PN(high He, N abundance arising from a higher mass progenitor star [8]) with strong bipolar symmetry; the color image, a combination of the emission in the lines of [O III], [O I], Hα, [N II], and [S II], shows the fine scale (dust) extinction features throughout the nebula. In contrast, NGC 6563 is an elliptical shell PN with a classical inner

high ionization zone and lower ionization shell, projected on a dense stellar field; NGC 6563 shows a fragmented CO emission shell [9].

Figure 1. Left: ESO press release images (eso1724) of the bipolar Galactic PN IC 4406 (left, image size $83 \times 83''$, north to upper left, east to lower left) and the elliptical PN NGC 6563 (right, image size $62 \times 62''$, north to the top), both taken with MUSE as part of the commissioning of the wide field mode with (ground layer) AO correction. The emission line images are color coded according to: [O III] blue; [O I] magenta; Hα green; [N II] orange; [S II] red. Image credits. IC 4406: ESO/J. Richard (CRAL); NGC 6563: ESO/P. Weilbacher (AIP).

4. MUSE Mapping of NGC 3132 and NGC 7009

The medium ionization PN, NGC 7009 (Saturn Nebula), was selected as a Science Verification target for MUSE in 2014 primarily on account of its size, which fits inside the MUSE field of view, the very high emission line surface brightness, and the availability of a wealth of previous observations, including Hubble Space Telescope (HST) imaging [10] and deep spectroscopy [4,5]. NGC 3132 was selected from among the MUSE PN observations during early commissioning for detailed analysis; on account of its larger projected elliptical form (dimensions $\sim 60 \times 85''$), a mosaic of MUSE pointings was performed to cover the optical emission extent. The ionization level of NGC 3132 is moderate with weak He II emission, but the central object is a wide visual binary with an A-type central star companion to the hot post-AGBstar [11].

The data for both nebulae were similarly reduced and for NGC 3132 with larger offsets to cover a full field of $124 \times 60''$; the sky background was estimated from the corners of the field and with a position well offset from any nebula halo emission. Emission lines were extracted from as many spaxels as possible given a signal-to-noise criterion and fitting multiple Gaussian profiles (see [12,13] for details). Short and long exposures were treated separately since bright lines ([O III],4959,5007Å, Hα, etc.) were saturated on longer exposures, and even [O III]5007Å was saturated over the bright shell emission in NGC 7009 in 10s exposure. The fitted emission line fluxes were reconstructed into images, and Figure 2 shows as an example the Hβ and He II 5411Å images for NGC 7009, illustrating the difference in structure between low and high ionization species. (ESO Release eso1731 https://www.eso.org/public/news/eso1731/) shows a multi-line color composite image from these data, which can be compared to the HST image (NASA opo9738g https://www.spacetelescope.org/images/opo9738g/).
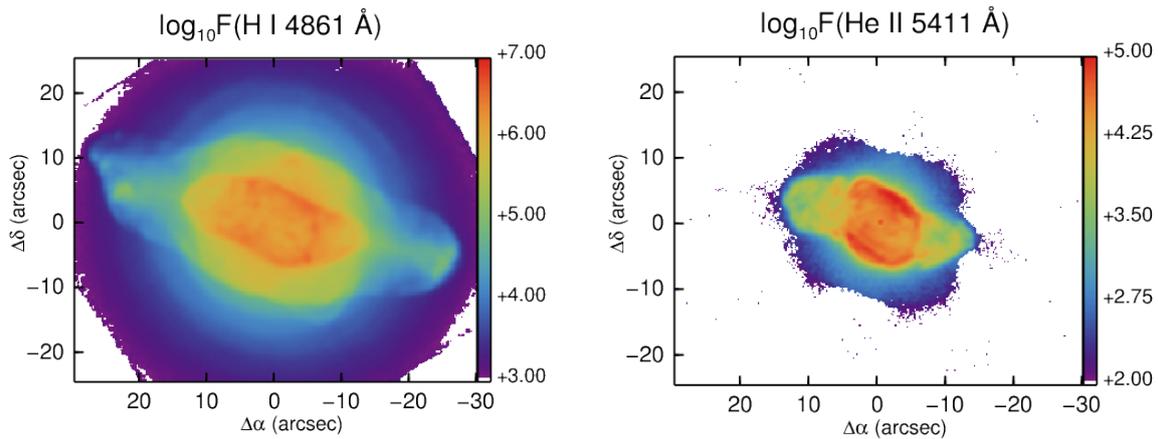
Figure 2. MUSE emission line images of NGC 7009: hydrogen Balmer Hβ 4861Å (left) and He II 5411Å 7–4 line (right), from [12].

4.1. Spectral Analysis: Line Ratios

For both nebulae, a common analysis was performed, and the following maps were derived:

- reddening from a ratio of Hα to Hβ (and also Paschen lines in the red, such as P10 (9015Å) and P9 (9229Å)) compared to Case B (nebula optically thick to HILyman-α photons; [14]);
- dereddened line maps (in absolute flux) for all measured lines;
- T_e from the [S III]6312/9068Å ratio, [N II]5755/6583Å and [O I]5577/6302Å for most spaxels, and from [Ar III]5192/7135Å in brighter regions (PyNeb [15] was used for nebular diagnostic computations);
- N_e from [Cl III]5517/5537Å and [S II]6716/6731Å;
- T_e from He I line ratios together with 3889Å optical depth;
- N_e from the ratio among the high series Paschen lines;
- T_e from the magnitude of the Paschen jump at 8210Å with respect to HI P11 (8863Å) line strength;
- ionic abundances of many species using the appropriate N_e, T_e diagnostics, such as O^+ and O^{++}, S^+ and S^{++}, and Ar^{++} and Ar^{+++};
- total abundances of He and O.

For both nebulae, although these diagnostics are standard, MUSE allows for the first time large field, high fidelity spatial mapping of their variation across the projected nebula surface.

Whilst it is difficult to compare distinct PNe, with a sample of only two, and chosen with diverse criteria, several points of similarity, which arise directly from the IFU spectroscopy, can be selected by a comparison of the results presented in [12,13,16]:

- The logarithmic extinction maps, $c(H\beta)$, show distinct features over the nebulae pointing to the presence of dust within the ionized regions (see Figure 3 and [16]). Whilst not unexpected, since some evidence of spatial extinction has been observed in the optical for a few PNe to date and dust emission detectable in the infrared is almost ubiquitous (e.g., [17]), the association of dust with distinct features of the nebular structure, such as shell edges, knots, etc., is noteworthy;
- T_e measured from the ratio of He I lines, or from the magnitude of the Paschen continuum jump at 8210Å, can be compared with the Collisionally Excited Line (CEL) T_e from the [S III] line ratio, to determine a CEL to recombination line temperature difference. In both NGC 7009 and NGC 3132, the difference in T_e increases towards the central star (see Figure 4). The radial trend of this increase is in the same sense as the increase of the Abundance Discrepancy Factor (ADF) measured between ORL and CEL abundances, for example for O^+ [18], although not yet in the same nebulae;

- The maps of total O abundance (i.e., O/H), derived on various assumptions of Ionization Correction Factor (ICF) to correct for the fact that [O IV] emission is not observed in the optical, is not flat for NGC 3132 or NGC 7009 ([12,13], as would be expected from evolutionary considerations (short-term alterations in O are not predicted in the late stages of low mass star evolution). The deviations from flatness in the O/H maps imply that the ICF procedure is incomplete: Figure 13 for NGC 3132 [13] and 21 for NGC 7009 [12] demonstrate that these O abundance modulations are correlated with the main shells and/or ionization zones.
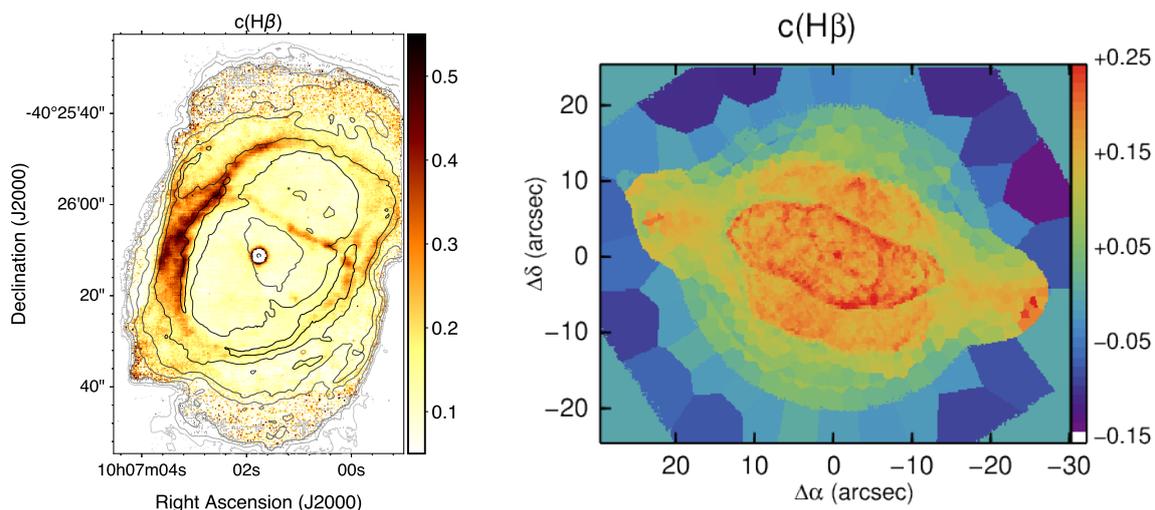
Figure 3. Comparison of the extinction, $c(H\beta)$, maps of NGC 3132 (left, from [13]) and NGC 7009 (right, from [16]) showing strong evidence for internal dust structures obscuring background emission. The NGC 3132 image is produced in the native spaxel format, whilst the $c(H\beta)$ image for NGC 7009 is produced from the ratio of Hα and Hβ images, which have been Voronoi tessellated to a constant signal-to-noise on Hβ flux.
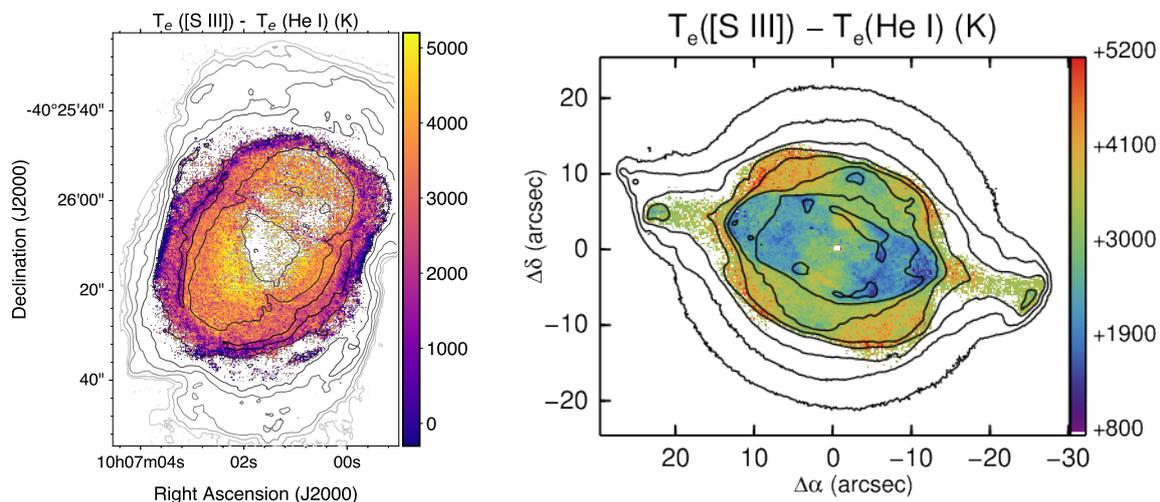
Figure 4. Comparison of the difference in T_e between the [S III] and He I T_e's in NGC 3132 (left [13]) and NGC 7009 (right [12]). An increasing trend (larger difference between T_e from [S III] and He I) is found in both nebulae towards the location of the central star within the main shell.

4.2. Spectral Analysis: Radial Velocities

Emission line profiles in PNe are broadened locally by thermal and turbulent velocities and globally by the nebular expansion (typically 15–40 km^{-1}); thus, the line profiles of metal lines have intrinsic widths of typically 10–20 kms^{-1}, while the H and He lines are broader. Although the

resolution of MUSE spectra is intermediate, around 2.7Å (velocity resolution 170–85 kms^{-1} from blue to red), some limited velocity information can be determined from Gaussian fitting of the lines. In [13], the velocity field of NGC 3132 was measured from several lines and showed a trend from higher to lower velocities from NW to SE; this trend was better seen in the forbidden lines and for the lower ionization lines of [N II] and [O I], but the behavior in the lower ionization species was more complex with both receding and approaching velocities in both lobes. A simple expanding shell seems difficult to reconcile with the pattern of velocities, and the velocity field could fit much better in a diabolo model, as proposed in [19].

5. Prospects

MUSE has great potential for moving spatial spectroscopic studies of PNe to a higher level, beyond the existing methods of slit-scanning and narrow band imaging, to high fidelity mapping of the full extent of the nebulae from the highest ionization regions near the central star to the neutral outer regions. There is also great potential for the discovery of additional domains in PNe, such as the Low Ionization Structure (LIS) regions found in at the extremities of NGC 3132 [13], where a mix of photoionization and shock excitation and abundance imprints of distinct late-stage stellar ejecta may exist.

Given the already substantial set of PNe observed with MUSE (Table 2), covering a wide range in central star temperature, morphology, and ADF, comparative studies can be initiated to explore correlations between diagnostics. Such a database can enable improvements in the domain of different CEL ratios for N_e, T_e measurement, with the impetus for improvement of atomic data where clear discrepancies arise. With a large set of empirical line ratios, diagnostics, and abundances, covering a diverse set of PNe, improvements in ICF's are enabled with implications for all targets of nebular spectroscopy.

The intermediate spectral resolution and lack of blue response of MUSE (Section 2) will be compensated by BlueMUSE [20], with coverage to 3500Å at a resolving power of >4000, which is a proposed instrument for the VLT in the 2020s. BlueMUSE brings several strategic advantages for the study of PNe: the availability of the auroral [O III]4363Å line for T_e measurement from the 4363/5007Å ratio for the bulk ionization stage of the dominant nebular coolant; coverage of the strong [O II]3726,3729Å doublet for the N_e and O$^+$ fraction; coverage and higher spectral resolution for measuring the weak O and C ORLs, enabling the spatial mapping of the ADF, at least for O.

References

1.　Bacon, R.; Accardo, M.; Adjali, L.; Anwand, H.; Bauer, S.; Biswas, I.; Blaizot, J.; Boudon, D.; Brau-Nogue, S.; Brinchmann, J.; et al. The MUSE second-generation VLT instrument. *Soc. Photo-Opt. Instrum. Eng. SPIE Conf. Ser.* **2010**, *7735*, 773508. [CrossRef]

2.　Richard, J.; Bacon, R. *MUSE User Manual, Version 9.1*; ESO: Garching, Germany, 2019.

3.　Dopita, M.A.; Ali, A.; Sutherland, R.S.; Nicholls, D.C.; Amer, M.A. IFU spectroscopy of southern planetary nebulae IV: A physical model for IC 418. *Mon. Not. R. Astron. Soc.* **2017**, *470*, 839–864. [CrossRef]

4.　Fang, X.; Liu, X.W. Very deep spectroscopy of the bright Saturn nebula NGC 7009—I. Observations and plasma diagnostics. *Mon. Not. R. Astron. Soc.* **2011**, *415*, 181–198. [CrossRef]

5.　Fang, X.; Liu, X.W. Very deep spectroscopy of the bright Saturn nebula NGC 7009—II. Analysis of the rich optical recombination spectrum. *Mon. Not. R. Astron. Soc.* **2013**, *429*, 2791–2851. [CrossRef]

6. García-Rojas, J.; Madonna, S.; Luridiana, V.; Sterling, N.C.; Morisset, C.; Delgado-Inglada, G.; Toribio San Cipriano, L. s-process enrichment in the planetary nebula NGC 3918. Results from deep echelle spectrophotometry. *Mon. Not. R. Astron. Soc.* **2015**, *452*, 2606–2640. [CrossRef]

7. Zhang, Y.; Liu, X.W.; Wesson, R.; Storey, P.J.; Liu, Y.; Danziger, I.J. Electron temperatures and densities of planetary nebulae determined from the nebular hydrogen recombination spectrum and temperature and density variations. *Mon. Not. R. Astron. Soc.* **2004**, *351*, 935–955. [CrossRef]

8. Peimbert, M.; Torres-Peimbert, S. Type I planetary nebulae. In *Planetary Nebulae*; Aller, L.H., Ed.; IAU Symposium; Reidel: Dordrecht, The Netherlands, , 1983; Volume 103, pp. 233–242.

9. Cox, P.; Huggins, P.J.; Bachiller, R.; Forveille, T. CO in the southern planetary nebulae NGC 6072, NGC 6563, and IC 4406. *Astron. Astrophys.* **1991**, *250*, 533.

10. Balick, B.; Alexander, J.; Hajian, A.R.; Terzian, Y.; Perinotto, M.; Patriarchi, P. FLIERs and Other Microstructures in Planetary Nebulae. IV. Images of Elliptical PNs from the Hubble Space Telescope. *Astron. J.* **1998**, *116*, 360–371. [CrossRef]

11. Ciardullo, R.; Bond, H.E.; Sipior, M.S.; Fullton, L.K.; Zhang, C.Y.; Schaefer, K.G. A HUBBLE SPACE TELESCOPE Survey for Resolved Companions of Planetary Nebula Nuclei. *Astron. Astrophys.* **1999**, *118*, 488–508. [CrossRef]

12. Walsh, J.R.; Monreal-Ibero, A.; Barlow, M.J.; Ueta, T.; Wesson, R.; Zijlstra, A.A.; Kimeswenger, S.; Leal-Ferreira, M.L.; Otsuka, M. An imaging spectroscopic survey of the planetary nebula NGC 7009 with MUSE. *Astron. Astrophys.* **2018**, *620*, A169. [CrossRef]

13. Monreal-Ibero, A.; Walsh, J.R. The MUSE view of the planetary nebula NGC 3132. *Astron. Astrophys.* **2020**, *634*, A47. [CrossRef]

14. Osterbrock, D.E.; Ferland, G.J. *Astrophysics of Gaseous Nebulae and Active Galactic Nuclei*; University Science Books: Sausalito, CA, USA, 2006.

15. Luridiana, V.; Morisset, C.; Shaw, R.A. PyNeb: A new tool for analyzing emission lines. I. Code description and validation of results. *Astron. Astrophys.* **2015**, *573*, A42. [CrossRef]

16. Walsh, J.R.; Monreal-Ibero, A.; Barlow, M.J.; Ueta, T.; Wesson, R.; Zijlstra, A.A. The extinction and dust-to-gas structure of the planetary nebula NGC 7009 observed with MUSE. *Astron. Astrophys.* **2016**, *588*, A106. [CrossRef]

17. Bernard-Salas, J. Infrared spectroscopy of planetary nebulae, including Spitzer. In *Planetary Nebulae in our Galaxy and Beyond*; Barlow, M.J., Méndez, R.H., Eds.; IAU Symposium; Cambridge University Press: Cambridge, UK, 2006; Volume 234, pp. 181–188. [CrossRef]

18. Wesson, R.; Jones, D.; García-Rojas, J.; Boffin, H.M.J.; Corradi, R.L.M. Confirmation of the link between central star binarity and extreme abundance discrepancy factors in planetary nebulae. *Mon. Not. R. Astron. Soc.* **2018**, *480*, 4589–4613. [CrossRef]

19. Monteiro, H.; Morisset, C.; Gruenwald, R.; Viegas, S.M. Morphology and Kinematics of Planetary Nebulae. II. A Diabolo Model for NGC 3132. *Astrophys. J.* **2000**, *537*, 853–860. [CrossRef]

20. Richard, J.; Bacon, R.; Blaizot, J.; Boissier, S.; Boselli, A.; Bouché, N.; Brinchmann, J.; Castro, N.; Ciesla, L.; Crowther, P. BlueMUSE: Project Overview and Science Cases. *arXiv* **2019**, arXiv:1906.01657.